

Dynamic recrystallization model of the Cu–Cr–Zr–Ag alloy under hot deformation

Yi Zhang^{a)} and Baohong Tian

School of Materials Science and Engineering, Henan University of Science and Technology, Luoyang 471003, China; and Collaborative Innovation Center of Nonferrous Metals, Henan University of Science and Technology, Henan Province, Luoyang 471003, China

Alex A. Volinsky^{b)}

Department of Mechanical Engineering, University of South Florida, Tampa 33620, USA

Xiaohong Chen

School of Materials Science and Engineering, University of Shanghai for Science and Technology, Shanghai 200093, China

Huili Sun

School of Materials Science and Engineering, Henan University of Science and Technology, Luoyang 471003, China; and Collaborative Innovation Center of Nonferrous Metals, Henan University of Science and Technology, Henan Province, Luoyang 471003, China

Zhe Chai

School of Materials Science and Engineering, Henan University of Science and Technology, Luoyang 471003, China; and School of Materials Science and Engineering, University of Shanghai for Science and Technology, Shanghai 200093, China

Ping Liu

School of Materials Science and Engineering, University of Shanghai for Science and Technology, Shanghai 200093, China

Yong Liu

School of Materials Science and Engineering, Henan University of Science and Technology, Luoyang 471003, China; and Collaborative Innovation Center of Nonferrous Metals, Henan University of Science and Technology, Henan Province, Luoyang 471003, China

(Received 29 January 2016; accepted 21 March 2016)

Hot deformation and dynamic recrystallization (DRX) behavior of the Cu–Cr–Zr–Ag alloy were studied by hot compressive tests in the 650–950 °C temperature and 0.001–10 s⁻¹ strain rate ranges using Gleeble-1500D thermomechanical simulator. The activation energy of deformation was determined as $Q = 343.23$ kJ/mol by the regression analysis. The critical conditions, including the critical strain and stress, for the occurrence of DRX were determined based on the alloy strain hardening rate. The critical strain related to the onset of DRX decreases with temperature. The ratios of the critical to peak stress and critical to peak strain were also identified as 0.91 and 0.49, respectively. The evolution of DRX microstructure strongly depends on the deformation conditions in terms of temperature and strain rate. Dislocation generation and multiplication are the main hot deformation mechanisms for the alloy. The addition of Ag can refine the grain and effectively improve the DRX of the Cu–Cr–Zr alloy. It can also inhibit the growth of the DRX grains at 950 °C deformation temperature, making the microstructure much more stable.

I. INTRODUCTION

Cu–Cr–Zr alloys have been widely used for many electrical applications, such as integrated circuit lead frame materials, diverter target materials and railway contact wires due to their high strength, outstanding

electrical properties, thermal conductivity, excellent fatigue resistance, and formability.^{1–3} Multiple studies have been carried out on the Cu–Cr–Zr alloys, and most of them focused on improving physical and mechanical properties, such as ductility, thermal stability, fatigue resistance, recrystallization behavior after cold rolling, strength and conductivity.^{4–6} The dynamic recovery (DRV) and dynamic recrystallization (DRX) occurring during hot deformation processing are important for obtaining suitable microstructure, which can influence mechanical and functional properties of the material and

Contributing Editor: Jürgen Eckert

Address all correspondence to these authors.

^{a)}e-mail: zhshgu436@163.com

^{b)}volinsky@usf.edu

DOI: 10.1557/jmr.2016.140

enhance its applicability.^{7–9} There are some investigations of hot deformation of the Cu–Cr–Zr alloys. Ding et al.¹⁰ studied the Cu–0.6Cr–0.03Zr alloy and found that the DRX developed completely at 750 °C and 850 °C when the grain size increased with decreasing strain rate and increasing deformation temperature. Ji et al.¹¹ found that under the test condition the deformation activation energy of the Cu–0.36Cr–0.03Zr alloy was 432.6 kJ/mol, and an experimentally based constitutive model was developed to predict the flow stress of the alloy during high temperature deformation. Zhang et al.¹² found that the addition of Ce can improve the Cu–Cr–Zr alloy deformation activation energy during hot deformation. However, relations between the important points of the flow stress curves and the critical conditions for DRX initiation during hot working need further attention.

In this paper, the flow behavior, kinetic analysis, and DRX behavior of Cu–Cr–Zr–Ag alloys have been investigated by hot compression tests. The constitutive equations and hot deformation activation energy have been derived for the alloy. The critical conditions for DRX of the alloy were determined to describe the DRX behavior. The effects of deformation temperature and strain rate on the microstructure evolution of the alloy are also discussed.

II. EXPERIMENTAL DETAILS

The Cu–Cr–Zr–Ag alloy was prepared using pure Cu, Cr, Zr, and Ag by melting in a vacuum induction furnace in argon, and then cast into a low-carbon steel mold with Φ 83 mm \times 150 mm dimensions. The chemical composition in wt% of this alloy is: 0.8 Cr, 0.3 Zr, 0.2 Ag, and Cu balance. The ingot was homogenized at 930 °C for 2 h to remove the alloying elements segregation. Subsequently, the ingot was forged into 25 mm diameter bars. Finally, the forged bars were solution-treated at 900 °C for 1 h, followed by water quenching.

The compression specimens with the diameter of 8 mm and the length of 12 mm were machined with their cylinder axes parallel to the axial line direction of the bar. Hot compression tests were carried out using the Gleeble-1500D thermomechanical simulator (Data Sciences International, Inc., New Brighton, Minnesota) at a strain rate of 0.001–10 s^{−1} and deformation temperature of 650–950 °C. The specimens were heated to the deformation temperature at 5 °C/s heating rate. Before deformation, all specimens were kept at the deformation temperature for 180 s to ensure a uniform starting temperature and decrease the material anisotropy. The accuracy of temperature control was ± 0.5 °C. The yield stress standard deviation for the performed measurements was ± 3 MPa. The standard deviation meets the ASTM-E8 standard and the error bars for the yield stress are less than $\pm 1.5\%$. After compression testing, the specimens were immediately quenched by water. The deformed

specimens were sectioned through the longitudinal axis. All specimens were polished and then etched with a solution of FeCl₃ (5 g) + C₂H₅OH (85 mL) + HCl (10 mL). The microstructure was observed using OLYMPUS PMG3 optical microscope (Olympus Optical Co. Ltd., Tokyo, Japan). Transmission electron microscopy (TEM) samples were prepared using Gatan 691 ion beam thinner (Gatan, Inc., Pleasanton, California). The precipitated phase was characterized using JEM-2100 high resolution TEM (JEOL Ltd., Tokyo, Japan).

III. RESULTS AND DISCUSSION

A. Flow stress behavior

The true stress–true strain curves obtained for the Cu–Cr–Zr–Ag alloy at various strain rates and deformation temperatures are shown in Fig. 1. The flow stress increased with the strain rate and stress decreased with the deformation temperature. The flow stress rapidly increased to a maximum value at a certain strain, and then gradually decreased to a steady state value at higher temperature and lower strain rate. This result is characteristic for hot working accompanied by dynamic softening.¹³ It can be seen that a typical DRX behavior was observed at the deformation temperature of 950 °C in Fig. 1.

True stress–true strain curves show typical DRV behavior at lower temperature and higher strain rate. DRV phenomenon happens because the higher strain rate or lower temperature provides shorter time for energy accumulation and lower grain boundary mobility.¹⁴ The effect of work hardening is stronger than the effect of dynamic softening. Continuous strain hardening was observed at the deformation temperature of 650 °C in Fig. 1.

The variations in the peak stress (σ_p) at various temperatures and strain rates are shown in Fig. 2. The peak stress strongly depends on the strain rate and temperature. It can also be found that the peak stress increases with the increase of strain rate and the decrease of deformation temperature.

B. Activation energy and constitutive equation

In hot working, the activation energy is related to the hot deformation mechanisms, such as DRV, DRX, and grain growth through the Zener–Hollomon parameter.¹⁵ The critical conditions for DRX initiation can also be determined by the activation energy. The hyperbolic-sine Arrhenius equation is widely used to describe the effects of the deformation temperature, strain rate, and activation energy. It can be expressed as^{16–18}:

$$\dot{\epsilon} = A[\sinh(\alpha\sigma)]^n \exp\left(-\frac{Q}{RT}\right) \quad (1)$$

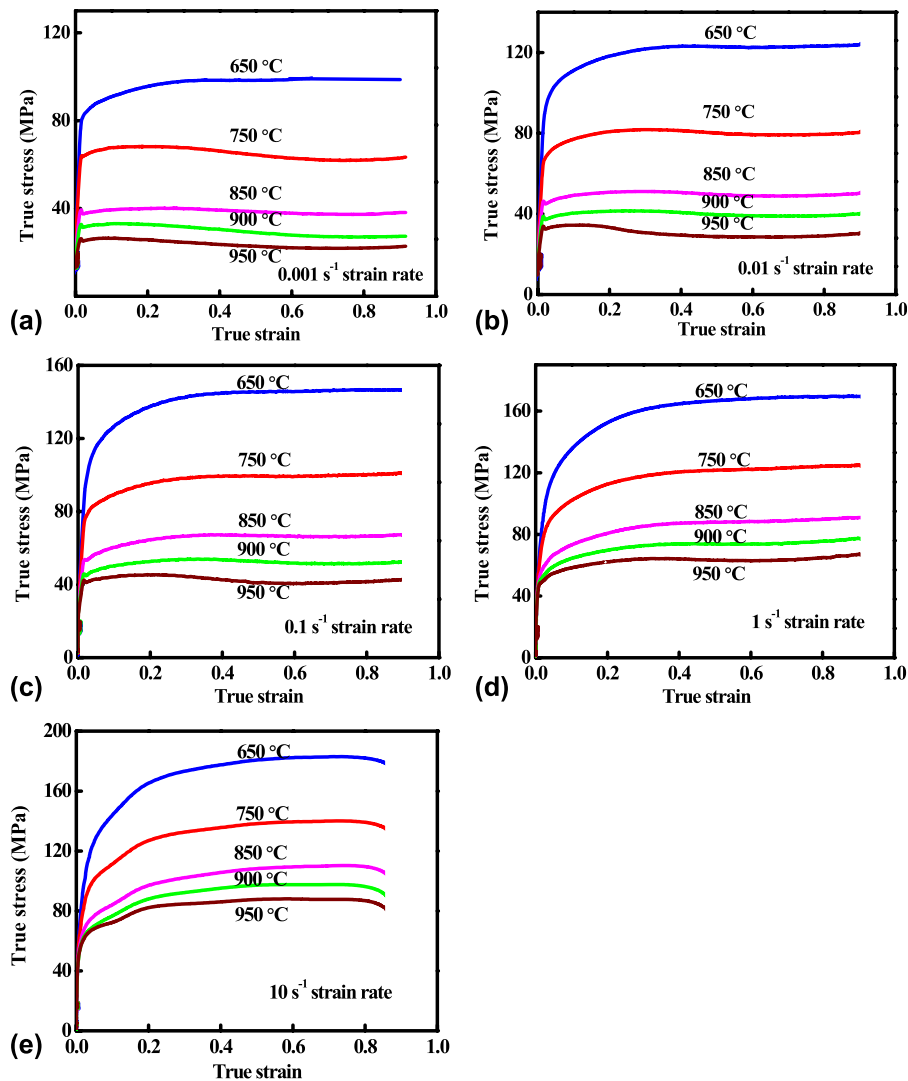


FIG. 1. True stress–strain curves of the Cu–Cr–Zr–Ag alloy under different deformation temperatures with strain rates: (a) $\dot{\epsilon} = 0.001 \text{ s}^{-1}$; (b) $\dot{\epsilon} = 0.01 \text{ s}^{-1}$; (c) $\dot{\epsilon} = 0.1 \text{ s}^{-1}$; (d) $\dot{\epsilon} = 1 \text{ s}^{-1}$; (e) $\dot{\epsilon} = 10 \text{ s}^{-1}$.

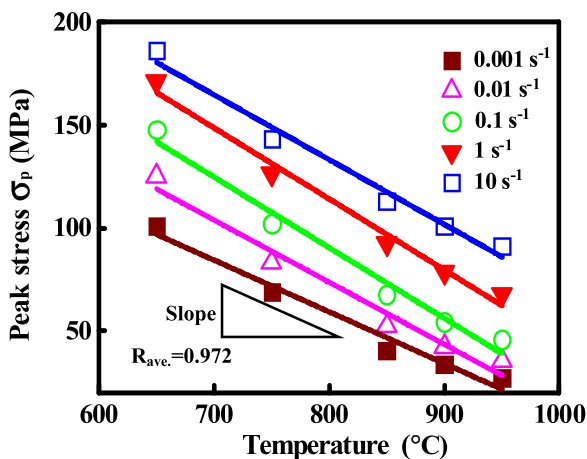


FIG. 2. Peak stress of the true stress–strain curves for the Cu–Cr–Zr–Ag alloy under different deformation conditions.

here, $\dot{\epsilon}$ is the strain rate (s^{-1}), Q is the activation energy of DRX (kJ/mol), R is the universal gas constant [8.314 J/(mol K)], T is the absolute temperature (K), σ is the flow stress (MPa) for a given stain, A (s^{-1}), n and α (MPa^{-1}) are the materials constants ($\alpha = \beta/n$). Taking natural logarithms of both sides of Eq. (1) yields:

$$\ln[\sinh(\alpha\sigma)] = \frac{1}{n} \ln \dot{\epsilon} + \frac{Q}{nR} \left(\frac{1}{T} \right) - \frac{1}{n} \ln A \quad (2)$$

The values of β and n at constant deformation temperature can be determined from the slope of the plots in Figs. 3(a) and 3(b) ($\ln \dot{\epsilon}$ versus σ and $\ln \dot{\epsilon}$ versus $\ln \sigma$). The corresponding average values are: $n = 10.24$, $\beta = 0.12$. Thus, the α value of the alloy is calculated as $\alpha = \beta/n = 0.012 \text{ MPa}^{-1}$.

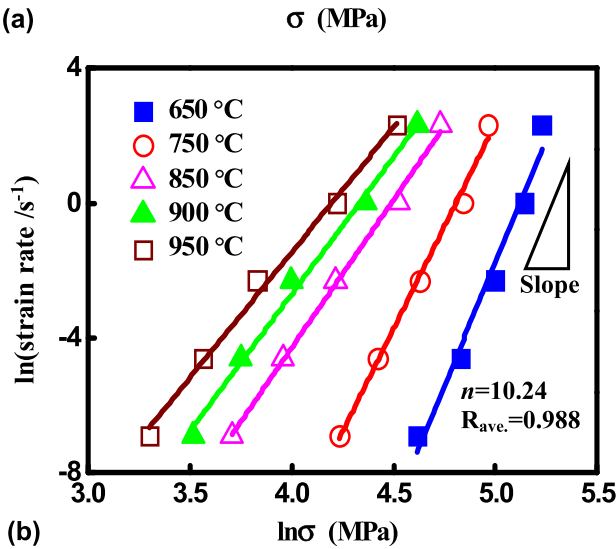
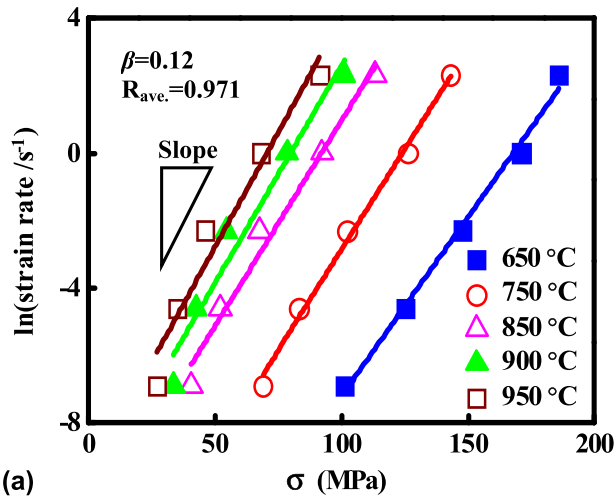


FIG. 3. Relationships between: (a) $\ln \dot{\epsilon}$ and σ ; (b) $\ln \dot{\epsilon}$ and $\ln \sigma$.

If $\dot{\epsilon}$ is a constant, Eq. (2) can be expressed as:

$$Q = R \left[\frac{\partial(\ln \dot{\epsilon})}{\partial \ln[\sinh(\alpha\sigma)]} \right]_T \left[\frac{\partial \ln[\sinh(\alpha\sigma)]}{\partial (1/T)} \right]_{\dot{\epsilon}} = Rn'S \quad (3)$$

Linear relationship between $\ln \dot{\epsilon} - \ln[\sinh(\alpha\sigma)]$ and $\ln[\sinh(\alpha\sigma)] - 1/T$ at different temperatures is evident in Figs. 4(a) and 4(b). The mean value of all the slopes in Fig. 4(a) is n' , and the mean value of all the slopes in Fig. 4(b) is S . The average slopes (n' and S) for the $\ln \dot{\epsilon} - \ln[\sinh(\alpha\sigma)]$ and $\ln[\sinh(\alpha\sigma)] - 1000/T$ plots are 7.72 and 5.35, respectively. Consequently, the value of Q for the experimental alloy is $Q = Rn'S = 343.23$ kJ/mol. The Q value of this alloy is a little lower than that of Cu–0.6Cr–0.03Zr alloy (572.053 kJ/mol), Cu–0.36Cr–0.03Zr alloy (432.6 kJ/mol), and Cu–0.8Cr–0.3Zr alloy (400.8 kJ/mol) compared with Refs. 10, 11 and 19, respectively. Compared with the above references, Ag has similar crystal structure and electro negativity to Cu. The grains of Cu–Cr–Zr alloy are refined by the addition of Ag.

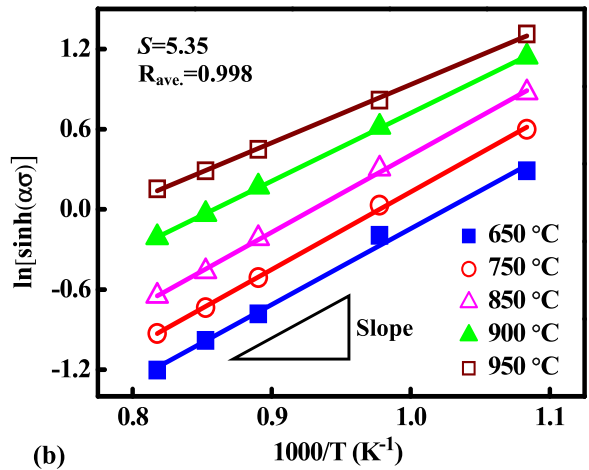
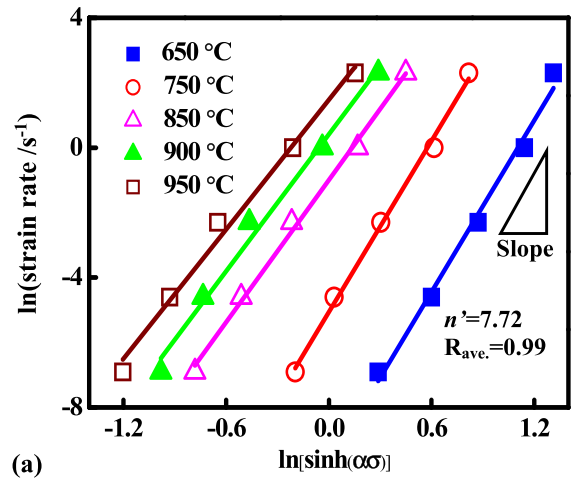


FIG. 4. Relationships between: (a) $\ln[\sinh(\alpha\sigma)]$ and $\ln \dot{\epsilon}$; (b) $\ln[\sinh(\alpha\sigma)]$ and $1000/T$.

Thus, the DRX nucleation is improved by the increase of grain boundary area due to the grain refinement effect with Ag addition. After that, the accumulated energy and the formation of dislocation density are increased by the addition of Ag. This also indicates that Ag addition can refine the grain and effectively fix dislocations at the grain boundaries and maintain high dislocation density. Finally, the driving force for recrystallized nucleation was improved. Therefore, the DRX is easier to occur for this experimental alloy. Ag addition will improve the DRX and optimize the hot workability of the Cu–Cr–Zr alloy.

The effects of temperature and strain rate on deformation behavior can be represented by a temperature-compensated strain rate factor, the Zener–Hollomon parameter, $Z^{20,21}$:

$$Z = \dot{\epsilon} \exp\left(\frac{Q}{RT}\right) = A[\sinh(\alpha\sigma)]^n \quad (4)$$

Taking natural logarithms of both sides of Eq. (4) yields:

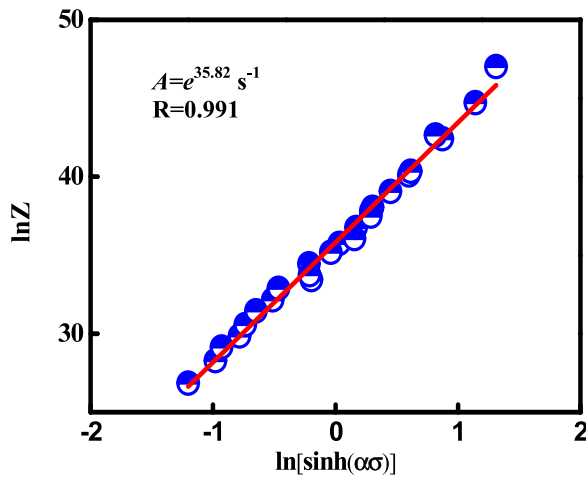


FIG. 5. The Zener–Hollomon parameter, Z , as a function of the flow stress.

$$\ln Z = \ln A + n \ln[\sinh(\alpha\sigma)] \quad (5)$$

Here, n is the stress index, and A is a material constant. Figure 5 illustrates the relationship between $\ln[\sinh(\alpha\sigma)]$ and $\ln Z$ for the Cu–Cr–Zr–Ag alloy. The plot exhibits linear correlation between the peak stress and the Z value with the regression coefficient of 0.99. The value of $n = 7.62$ is the slope and the value of $\ln A = 35.82$ is the intercept of the fitted curves in Fig. 5.

Thus, the constitutive equation of the Cu–Cr–Zr–Ag alloy in the hyperbolic-sine function can be expressed as:

$$\dot{\epsilon} = e^{35.82} [\sinh(0.012\sigma)]^{7.62} \exp\left(-\frac{343.23}{RT}\right) \quad (6)$$

C. Characteristic points of the flow curves

The critical strain (ϵ_c) of material is important for DRX research. The accurate and simple method to determine the critical strain for the initiation of DRX is derived from the flow curves.²² Poliak and Jonas²³ have shown that the inflection in $\ln \theta - \epsilon$ curves can be used to find the critical strain for the onset of DRX. The $\ln \theta - \epsilon$ curve and its corresponding third order polynomial for the Cu–Cr–Zr–Ag alloy deformed at the strain rate of 0.01 s^{-1} and varying temperature are shown in Fig. 6. The inflection point of the $\ln \theta - \epsilon$ curves is marked by an arrow in Fig. 6(a) and is clear for the critical strain ϵ_c of the alloy deformed at $950 \text{ }^\circ\text{C}$ with strain rate of 0.01 s^{-1} . The inflection point corresponds to the maximum value on the $-\partial(\ln \theta)/\partial\epsilon - \epsilon$ versus ϵ curve shown in Fig. 6(b). All the curves have clear inflection points in Fig. 6(a) and the critical strain in Fig. 6(b), which clearly indicate that DRX occurs at all deformation temperatures under the strain rate of 0.01 s^{-1} . The critical strain related to the onset of DRX decreases with temperature because it

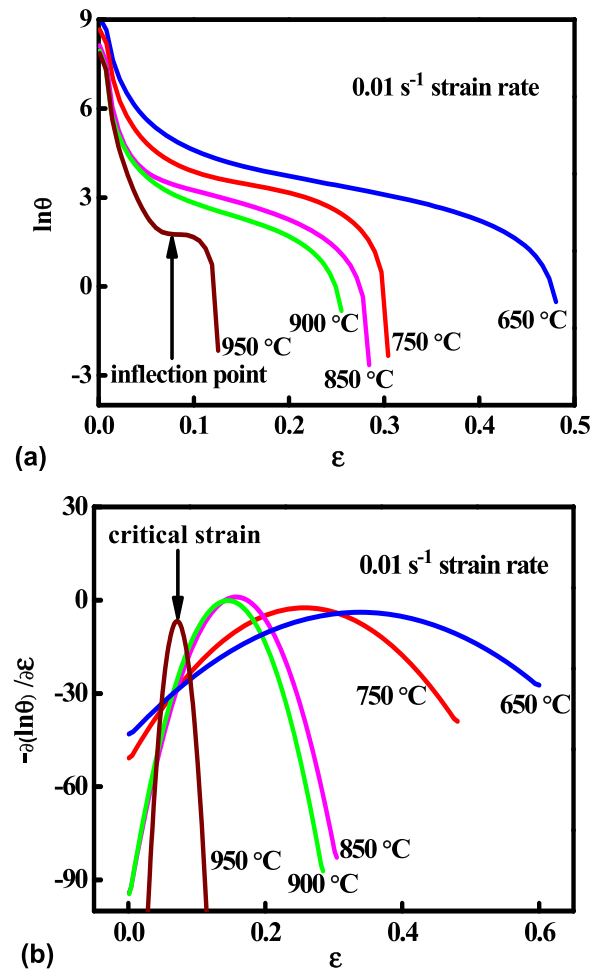


FIG. 6. (a) Relationship between $\ln \theta$ and ϵ ; (b) $-\partial(\ln \theta)/\partial\epsilon - \epsilon$ versus ϵ plots for the Cu–Cr–Zr–Ag alloy at different temperatures under the strain rate of 0.01 s^{-1} .

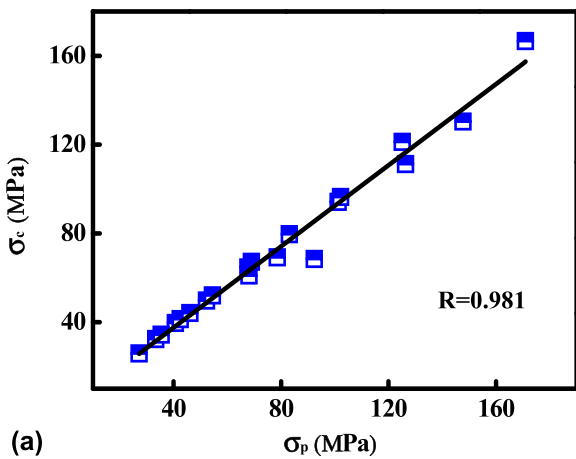
is a thermally activated process. The energy accumulated for the nucleation and growth of the DRX grains at lower temperature is insufficient.²⁴ Similar results were observed by Han et al.²⁵ for the 254SMO super-austenitic stainless steel and by Ji et al.²⁶ for the Cu–Mg alloys. The relationships between critical strain ϵ_c and peak strain ϵ_p , critical stress σ_c and peak stress σ_p are shown in Fig. 7. According to Figs. 7(a) and 7(b), the normalized critical strain and stress could be presented as:

$$\sigma_c/\sigma_p = 0.91 \quad (7)$$

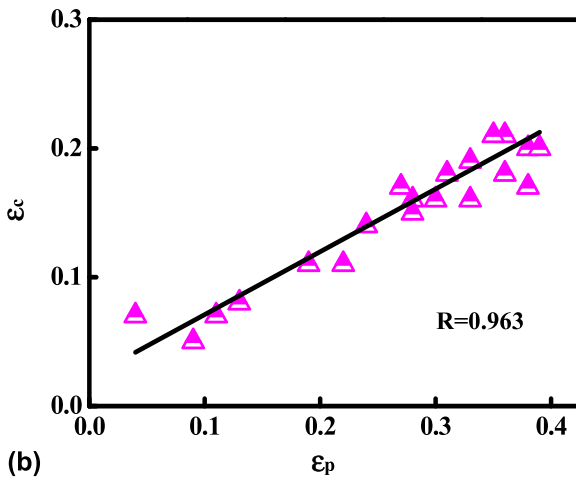
$$\epsilon_c/\epsilon_p = 0.49 \quad (8)$$

For a constant initial grain size, the relationship between peak strains ϵ_p and Z parameter can be expressed as²⁷:

$$\epsilon_p = KZ^m \quad (9)$$



(a)



(b)

FIG. 7. Relationships between: (a) σ_c and σ_p ; (b) ϵ_c and ϵ_p .

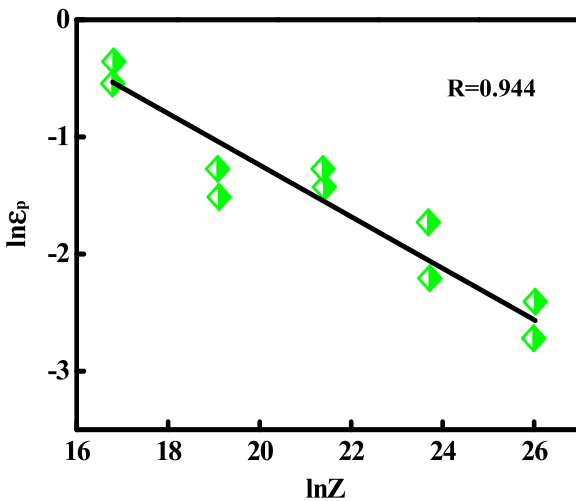


FIG. 8. Relationship between the Z parameter and the peak strain.

where K and m are material constants, dependent on the alloy composition. The relation between ϵ_p and Z is shown in Fig. 8. According to Fig. 8, the peak strain ϵ_p can be predicted using the following equation:

$$\epsilon_p = 23.7Z^{-0.22} \quad (10)$$

According to Eq. (8), the relationship between the critical strain ϵ_c and the Z parameter can be expressed as:

$$\epsilon_c = 11.61Z^{-0.22} \quad (11)$$

D. Microstructure evolution

Optical images of the Cu–Cr–Zr–Ag alloy microstructure deformed at the strain rate of 0.01 s^{-1} and different deformation temperature are shown in Fig. 9. The original grains are elongated along the deformation direction when deformed at $650 \text{ }^\circ\text{C}$, the average grain size is $20 \text{ }\mu\text{m}$ according to Fig. 9(a). The serrated grain boundaries marked by the arrows were observed in Fig. 9(b). It was generally considered as the features of the early DRX stage.²⁸ With increasing the deformation temperature, a large number of new DRX grains were nucleated at the original grain boundaries in Fig. 9(c). The average grain size was determined to be about $18 \text{ }\mu\text{m}$. It also can be seen that the typical necklace structure around the initial grain boundaries is present in Fig. 9(c). The occurrence of necklace structure indicates that the grain boundary bulging through strain-induced grain boundary migration is the dominant nucleation mechanism of DRX.²⁵ According to Fig. 9(d), the original grains were replaced entirely by the new DRX grains when the deformation temperature reached $900 \text{ }^\circ\text{C}$. This means that the full DRX has been achieved. The serrated grain boundaries were observed again in Fig. 9(e). The average DRX grain size of specimens deformed at $900 \text{ }^\circ\text{C}$ and $950 \text{ }^\circ\text{C}$ is $26 \text{ }\mu\text{m}$ and $33 \text{ }\mu\text{m}$, respectively. Thus, there is obvious grain coarsening, demonstrating that the grain size increased with the deformation temperature. The reasons for such phenomenon are grain boundary migration and grain growth processes. According to the above analysis, it can be concluded that the evolution of DRX microstructure strongly depends on the deformation conditions (temperature and strain rate).

Figure 10 shows TEM micrographs of the Cu–Cr–Zr–Ag alloy deformed at different conditions. The banded structures were observed in Fig. 10(a) deformed at $650 \text{ }^\circ\text{C}$ and 0.01 s^{-1} . Figure 10(b) shows that the dislocations are tangled and stored in the grains interior of the Cu–Cr–Zr–Ag alloy deformed at $750 \text{ }^\circ\text{C}$ with the 0.01 s^{-1} strain rate. The dislocation climb and cross-slip in low stacking fault energy alloy are difficult at low deformation temperature. Thus, the high density dislocations are intersected and tangled, forming the network structure, which makes dislocation slip more difficult.²⁹ The increase of the number of

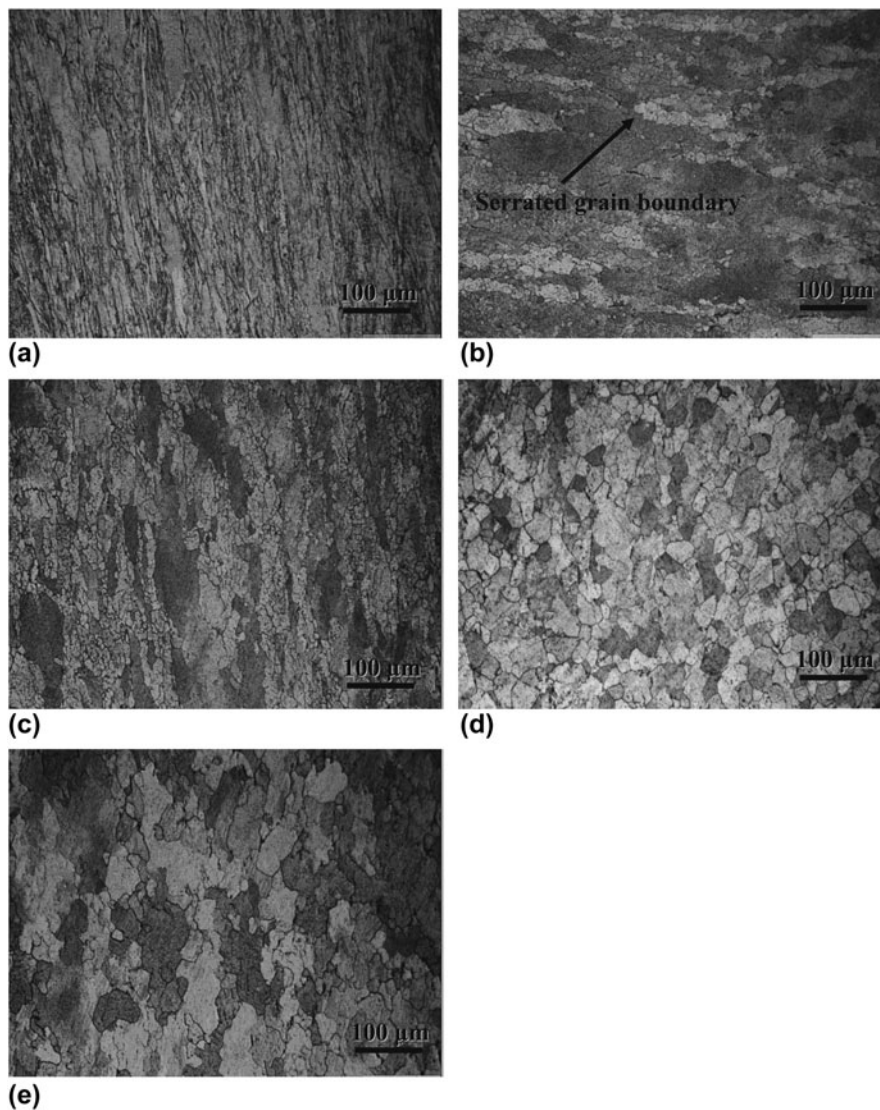


FIG. 9. Optical images of the deformed microstructure of the hot compressed specimens at a strain rate of 0.01 s^{-1} and various temperatures: (a) $650 \text{ }^\circ\text{C}$; (b) $750 \text{ }^\circ\text{C}$; (c) $850 \text{ }^\circ\text{C}$; (d) $900 \text{ }^\circ\text{C}$ and (e) $950 \text{ }^\circ\text{C}$.

dislocations is observed in Figs. 10(c) and 10(d) for the alloy deformed at $800 \text{ }^\circ\text{C}$ and $850 \text{ }^\circ\text{C}$ with the 0.1 s^{-1} strain rate. Compared with Fig. 10(b), the dislocation density is much higher in Figs. 10(c) and 10(d). According to the calculation from the selected area electron diffraction (SAED) patterns, the interplanar spacing in Fig. 10(d) is much higher than in Fig. 10(c). It also indicates that the dislocation density is much higher in Fig. 10(d). The rapid increase of the number of dislocations easily induces DRX once the dislocation density exceeds a critical value.³⁰ When the alloy deformed at $850 \text{ }^\circ\text{C}$ and 0.001 s^{-1} , the nucleation of dynamically recrystallized grains appears at the high-angle grain boundaries marked by arrow in Fig. 10(e), which indicates the DRX occurrence. That is because the activation of dislocation movement accelerates the

dislocation annihilation rate when the alloy is deformed at higher temperature.

IV. DISCUSSION

Figure 11(a) and 11(b) show the microstructure of the Cu–Cr–Zr and Cu–Cr–Zr–Ag alloys after solution treatment. Evidently, the addition of Ag can refine the grains of the base Cu–Cr–Zr alloy. The grain size of the Cu–Cr–Zr–Ag alloy is considerably smaller than the Cu–Cr–Zr alloy. The average grain size of the Cu–Cr–Zr and Cu–Cr–Zr–Ag alloys is approximately $69 \text{ }\mu\text{m}$ and $58 \text{ }\mu\text{m}$, respectively. Grain refinement may be attributed to the enrichment of Ag atoms in front of the solid–liquid interface during solidification. To compare the microstructures of the Cu–Cr–Zr and Cu–Cr–Zr–Ag alloys

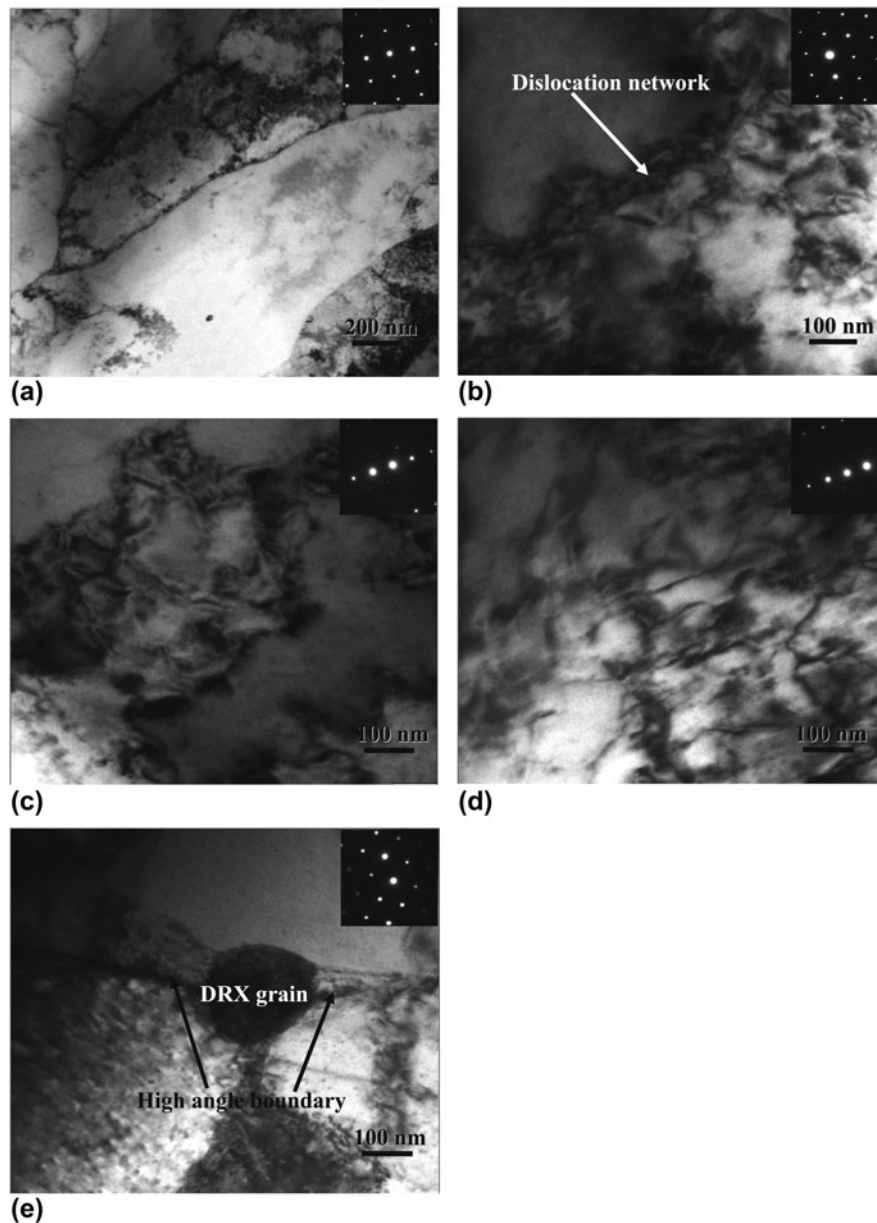


FIG. 10. TEM micrographs of the Cu–Cr–Zr–Ag alloy deformed at different deformation temperatures and strain rates: (a) 650 °C, 0.01 s⁻¹; (b) 750 °C, 0.01 s⁻¹; (c) 800 °C, 0.1 s⁻¹; (d) 850 °C, 0.1 s⁻¹; (e) 850 °C, 0.001 s⁻¹.

during hot deformation, the deformation microstructures of the two alloys deformed at the strain rate of 0.001 s⁻¹ and different temperatures are shown in Fig. 12, respectively. It can be seen that the elongated grains are found in Fig. 12(a), with a mean grain size of 31 μm. This means that the main softening mechanism is DRV for the Cu–Cr–Zr alloy deformed at 650 °C and 0.001 s⁻¹. The elongated grains are also observed for the Cu–Cr–Zr–Ag alloy deformed at 650 °C and 0.001 s⁻¹, as seen in Fig. 12(c). Compared with the Cu–Cr–Zr–Ag alloy deformed at the same conditions, the average grain size is 26 μm. When the deformation temperature increased to 850 °C at the same strain rate of 0.001 s⁻¹, the original

grains were elongated along the deformation direction and the average grain size was 16 μm, as seen in Fig. 12(b). Compared with the Figs. 12(a) and 12(b), some new fine DRX were found at the previous grain boundaries, so this structure is often called typical necklace-type structure by some researchers.³¹ This demonstrates that the DRX occurs at these deformation conditions. According to Fig. 12(d), large number of smaller and uniform DRX grains was obtained. Completed DRX for the Cu–Cr–Zr–Ag alloy is observed at the 850 °C deformation temperature and 0.001 s⁻¹ strain rate. The minimal average grain size is achieved at these deformation conditions, which is about 11 μm.

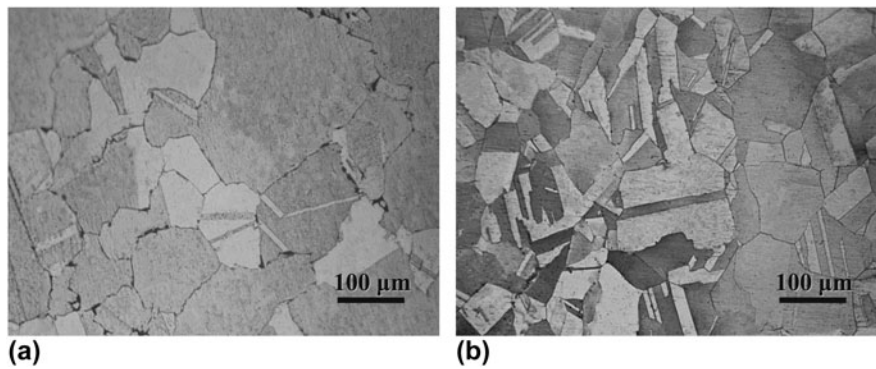


FIG. 11. Microstructure of (a) Cu–Cr–Zr and (b) Cu–Cr–Zr–Ag alloys after solution treatment at 900 °C for 1 h.

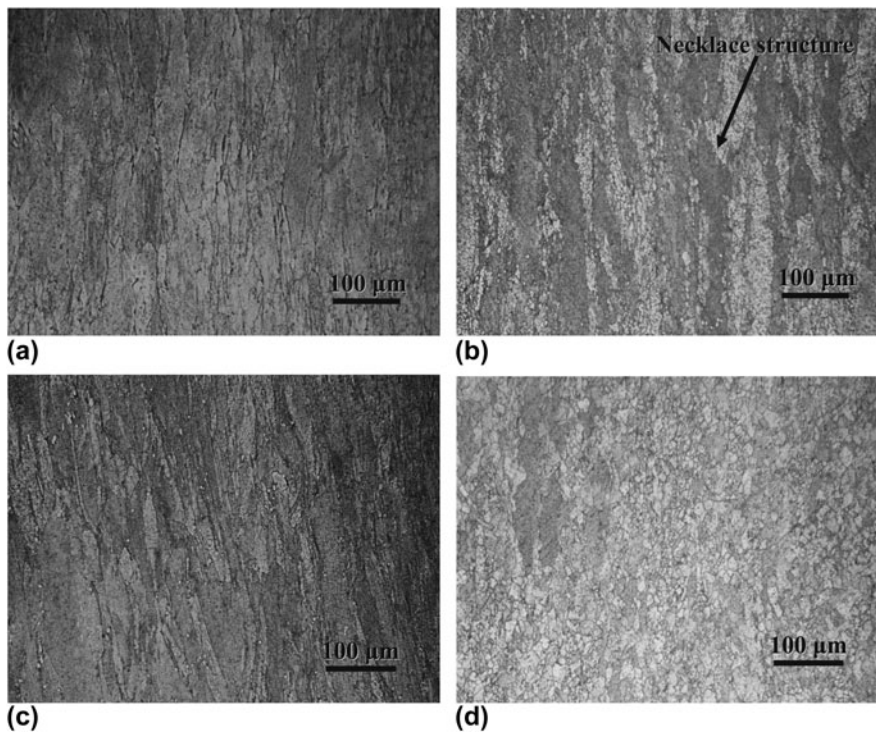


FIG. 12. Microstructure of (a and b) Cu–Cr–Zr and (c and d) Cu–Cr–Zr–Ag alloys hot deformed at: (a) 650 °C and 0.001 s^{-1} ; (b) 850 °C and 0.001 s^{-1} ; (c) 650 °C and 0.001 s^{-1} ; (d) 850 °C and 0.001 s^{-1} .

Compared with Figs. 12(b) and 12(d), the original grains were replaced completely by new fine DRX grains. This means that the addition of Ag can effectively refine the grain and improve dynamic recrystallization. The reasons for this is that the boundary areas can increase by the addition of Ag, and then the boundary movement and grain rotation can be promoted because of the fine recrystallized grains during the hot deformation.³² Therefore, a mass of dislocations pile up during hot deformation. TEM micrographs of the Cu–Cr–Zr and Cu–Cr–Zr–Ag alloy deformed at different conditions are shown in Figs. 13(a) and 13(b), respectively. It can be seen that the dislocation density is increased by the addition of Ag, for the two

alloy deformed at the same condition. Finally, the driving force of recrystallized nucleation was improved by high dislocation density.

Completely formed DRX grains for the Cu–Cr–Zr alloy are shown in Fig. 14(a). The measured dynamically recrystallized grain size deformed at 950 °C and 1 s^{-1} is 26 μm. With the decreasing strain rate, a little coarser DRX grains with an average grain size of 32 μm are obtained in Fig. 14(b) compared with Fig. 14(a). Compared with the Cu–Cr–Zr–Ag alloy deformed at 950 °C and 1 s^{-1} , much smaller DRX grains are observed in Fig. 14(c) with the mean grain size of 17 μm. The completely recrystallized uniform and fine grains are shown in Fig. 14(d). Moreover, the grain size changed

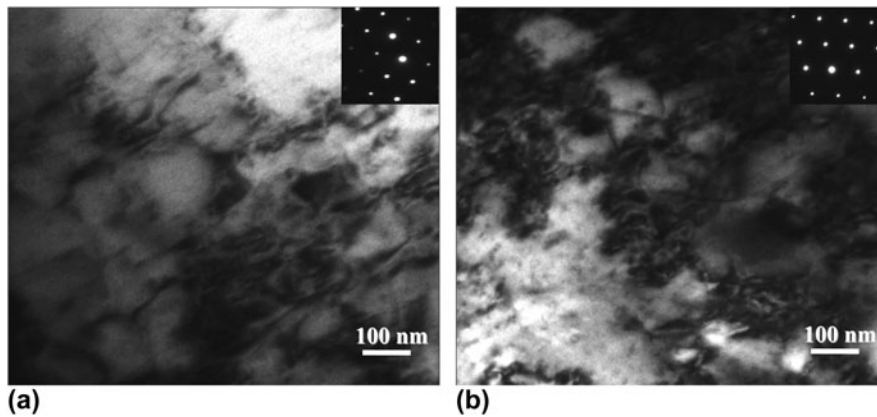


FIG. 13. TEM micrographs of the (a) Cu–Cr–Zr and (b) Cu–Cr–Zr–Ag alloy deformed at 850 °C and 0.01 s^{-1} .

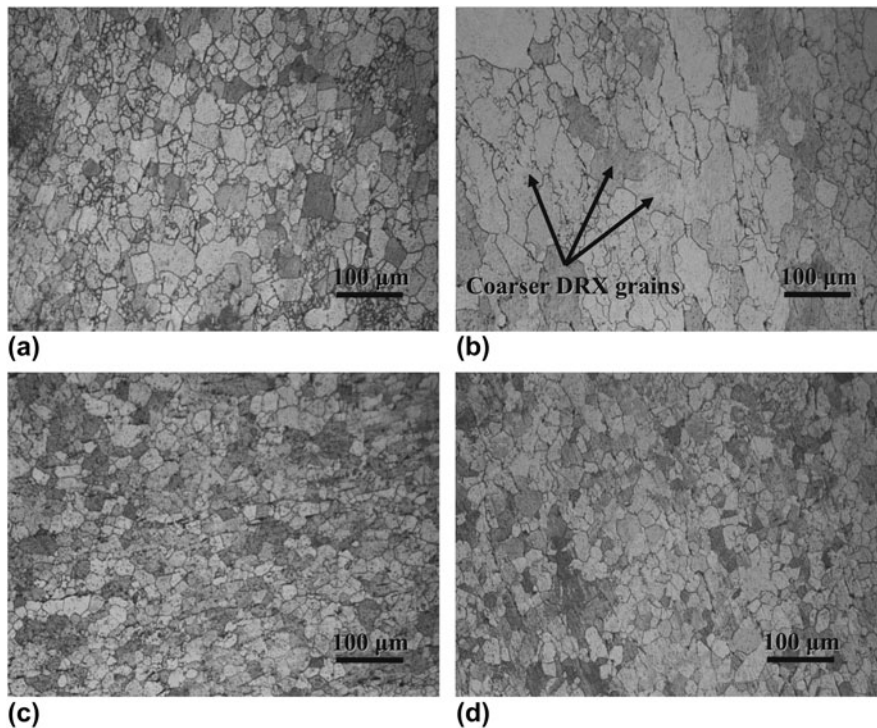


FIG. 14. Microstructure of (a and b) Cu–Cr–Zr and (c and d) Cu–Cr–Zr–Ag alloys hot deformed at: (a) 950 °C and 1 s^{-1} ; (b) 950 °C and 0.1 s^{-1} ; (c) 950 °C and 1 s^{-1} ; (d) 950 °C and 0.1 s^{-1} .

slightly from $17 \mu\text{m}$ deformed at 950 °C and 1 s^{-1} [Fig. 14(c)] to $20 \mu\text{m}$ deformed at 950 °C and 0.1 s^{-1} [Fig. 14(d)]. The grain size was quite similar for these two conditions because of no further recrystallization, even at lower strain rate. At the same time, the grain size is also much smaller compared with Fig. 14(b). This indicates that the addition of Ag can inhibit the growth of the DRX grains at the deformation temperature of 950 °C. Ag has much better high temperature stability than Cu at high temperature. Thus, Ag is distributed at the grain subgrain boundary. It can fix dislocations at the grain boundaries and maintain high dislocation density. From the above analysis, the addition of Ag can refine the

grain and improve dynamic recrystallization, and inhibit the growth of the DRX grains at very high deformation temperature. This is also very important for the alloy applications in industrial practice.

V. CONCLUSIONS

Hot deformation behavior of Cu–Cr–Zr–Ag alloy has been investigated at a temperature range of 650–950 °C and the strain rate range of $0.001\text{--}10 \text{ s}^{-1}$. The following conclusions can be drawn:

(1) The flow stress increases with the strain rate and stress decreases with the deformation temperature.

(2) The activation energy of deformation was calculated to be $Q = 343.23$ kJ/mol by the regression analysis. The constitutive equation for the flow stress can be expressed as: $\dot{\varepsilon} = e^{35.82} [\sinh(0.012\sigma)]^{7.62} \exp\left(-\frac{343.23}{RT}\right)$.

(3) The critical strain related to the onset of DRX decreases with deformation temperature. The critical ratios of σ_c/σ_p and $\varepsilon_c/\varepsilon_p$ are identified as 0.91 and 0.49, respectively. The relation between ε_p , ε_c and Z were derived as: $\varepsilon_p = 23.7Z^{-0.22}$, $\varepsilon_c = 11.61Z^{-0.22}$, respectively.

(4) The evolution of DRX microstructure strongly depends on the deformation conditions (temperature and strain rate). The deformation temperature increase and the strain rate decrease can promote DRX of the Cu–Cr–Zr–Ag alloy.

(5) The addition of Ag can refine the grain and effectively accelerate dynamic recrystallization. It can also inhibit the growth of the DRX grains at the deformation temperature of 950 °C.

ACKNOWLEDGMENTS

This work was supported by the National Natural Science Foundation of China (51101052) and the National Science Foundation (IRES 1358088).

REFERENCES

- J.H. Su, Q.M. Dong, P. Liu, H.J. Li, and B.X. Kang: Research on aging precipitation in a Cu–Cr–Zr–Mg alloy. *Mater. Sci. Eng., A* **392**, 422 (2005).
- H.T. Tran, M.H. Shirangi, X. Pang, and A.A. Volinsky: Temperature, moisture and mode-mixity effects on copper leadframe/EMC interfacial fracture toughness. *Int. J. Fract.* **185**, 115 (2013).
- L.M. Bi, P. Liu, X.H. Chen, X.K. Liu, W. Li, and F.C. Ma: Analysis of phase in Cu–15%Cr–0.24%Zr alloy. *Trans. Nonferrous Met. Soc. China* **23**, 1342 (2013).
- G.B. Lin, Z.D. Wang, M.K. Zhang, H. Zhang, and M. Zhao: Heat treatment method for making high strength and conductivity Cu–Cr–Zr alloy. *Mater. Sci. Technol.* **27**, 966 (2011).
- Y. Pang, C.D. Xia, M.P. Wang, Z. Li, Z. Xiao, H.G. Wei, X.F. Sheng, Y.L. Jia, and C. Chen: Effects of Zr and (Ni, Si) additions on properties and microstructure of Cu–Cr alloy. *J. Alloys Compd.* **582**, 786 (2014).
- P. Liu, B.X. Kang, X.G. Cao, J.L. Huang, B. Yen, and H.C. Gu: Aging precipitation and recrystallization of rapidly solidified Cu–Cr–Zr–Mg alloy. *Mater. Sci. Eng., A* **265**, 262 (1999).
- Y.H. Kong, P.P. Chang, Q. Li, L.X. Xie, and S.G. Zhu: Hot deformation characteristics and processing map of nickel-based C276 superalloy. *J. Alloys Compd.* **622**, 738 (2015).
- A. Momeni and S.M. Abbasi: On the opposition of dynamic recrystallization and solute dragging in steels. *J. Alloys Compd.* **622**, 318 (2015).
- D.G. Cram, H.S. Zuro, Y.J.M. Brechet, and C.R. Hutchinson: Modelling discontinuous dynamic recrystallization using a physically based model for nucleation. *Acta Mater.* **57**, 5218 (2009).
- Z.Y. Ding, S.G. Jia, P.F. Zhao, M. Deng, and K.X. Song: Hot deformation behavior of Cu–0.6Cr–0.03Zr alloy during compression at elevated temperatures. *Mater. Sci. Eng., A* **570**, 87 (2013).
- G.L. Ji, Q. Li, K.Y. Ding, L. Yang, and L. Li: A physically-based constitutive model for high temperature deformation of Cu–0.36Cr–0.03Zr alloy. *J. Alloys Compd.* **648**, 397 (2015).
- Y. Zhang, A.A. Volinsky, H.T. Tran, Z. Chai, P. Liu, and B.H. Tian: Effects of Ce addition on high temperature deformation behavior of Cu–Cr–Zr alloys. *J. Mater. Eng. Perform.* **24**, 3783 (2015).
- A. Galiyev, R. Kaibyshev, and G. Gottstein: Correlation of plastic deformation and dynamic recrystallization in magnesium alloy ZK60. *Acta Mater.* **49**, 1199 (2001).
- D.J. Li, Y.R. Feng, S.Y. Song, Q. Liu, Q. Bai, F.Z. Ren, and F.S. Shangguan: Influences of silicon on the work hardening behavior and hot deformation behavior of Fe–25 wt%Mn–(Si, Al) TWIP steel. *J. Alloys Compd.* **618**, 768 (2015).
- I. Salvatori, T. Inoue, and K. Nagai: Ultrafine grain structure during dynamic recrystallization for type 304 stainless steel. *ISIJ Int.* **42**, 744 (2002).
- Y. Xu, L. Xi, and Y. Sun: Deformation behaviour and dynamic recrystallization of AZ61 magnesium alloy. *J. Alloys Compd.* **580**, 262 (2013).
- A. Dehghan-Manshadi, M.R. Barnett, and P.D. Hodgson: Hot deformation and recrystallization of austenitic stainless steel: Part I. Dynamic recrystallization. *Metall. Mater. Trans. A* **39**, 1359 (2008).
- G.Z. Quan, Y. Shi, Y.X. Wang, B.S. Kang, T.W. Ku, and W.J. Song: Constitutive modeling for the dynamic recrystallization evolution of AZ80 magnesium alloy based on stress–strain data. *Mater. Sci. Eng., A* **528**, 8051 (2011).
- Y. Zhang, Z. Chai, Q.Q. Xu, B.H. Tian, Y. Liu, and P. Liu: Hot deformation behavior and processing maps of Cu–0.8Cr–0.3Zr alloy. *Trans. Mater. Heat Treat.* **36**, 8 (2015).
- A. Etaati and K. Dehghani: A study on hot deformation behavior of Ni–42.5Ti–7.5Cu alloy. *Mater. Chem. Phys.* **140**, 208 (2013).
- G.Z. Quan, Y.P. Mao, G.S. Li, W.Q. Lv, Y. Wang, and J. Zhou: A characterization for the dynamic recrystallization kinetics of as-extruded 7075 aluminum alloy based on true stress–strain curves. *Comput. Mater. Sci.* **55**, 65 (2012).
- M.H. Wang, Y.F. Li, W.H. Wang, J. Zhou, and A. Chiba: Quantitative analysis of work hardening and dynamic softening behavior of low carbon alloy steel based on the flow stress. *Mater. Des.* **45**, 384 (2013).
- E.I. Poliak and J.J. Jonas: Initiation of dynamic recrystallization in constant strain rate hot deformation. *ISIJ Int.* **43**, 684 (2003).
- H.Y. Wu, J.C. Yang, J.H. Liao, and F.J. Zhu: Dynamic behavior of extruded AZ61 Mg alloy during hot compression. *Mater. Sci. Eng., A* **68**, 535 (2012).
- Y. Han, H. Wu, W. Zhang, D.N. Zou, G.W. Liu, and G.J. Qiao: Constitutive equation and dynamic recrystallization behavior of as-cast 254SMO super-austenitic stainless steel. *Mater. Des.* **69**, 230 (2015).
- G. Ji, Q. Li, and L. Li: The kinetics of dynamic recrystallization of Cu–0.4Mg alloy. *Mater. Sci. Eng., A* **586**, 197 (2013).
- S.M. Abbasi and A. Shokuhfar: Prediction of hot deformation behaviour of 10Cr–10Ni–5Mo–2Cu steel. *Mater. Lett.* **61**, 2523 (2007).
- D.J. Li, Y.R. Feng, Z.F. Yin, F.S. Shangguan, K. Wang, Q. Liu, and F. Hu: Prediction of hot deformation behaviour of Fe–25Mn–3Si–3Al TWIP steel. *Mater. Sci. Eng., A* **528**, 8084 (2011).
- D.X. Wen, Y.C. Lin, J. Chen, X.M. Chen, J.L. Zhang, Y.J. Li, and L.T. Liang: Work-hardening behaviors of typical solution-treated and aged Ni-based superalloys during hot deformation. *J. Alloys Compd.* **618**, 372 (2015).
- Q. Guo, H.G. Yan, Z.H. Chen, and H. Zhang: Grain refinement in as-cast AZ80 Mg alloy under large strain deformation. *Mater. Charact.* **58**, 162 (2007).
- S.L. Semiatin, D.S. Weave, R.C. Kram, P.N. Fagin, M.G. Glavicic, R. L. Goetz, N.D. Frey, and M.M. Antony: Deformation and recrystallization behavior during hot working of a coarse-grain, nickel-base superalloy ingot material. *Metall. Mater. Trans. A* **35**, 679 (2004).
- Y.Y. Chen, B.H. Li, and F.T. Kong: Effects of minor yttrium addition on hot deformability of lamellar Ti–45Al–5Nb alloy. *Trans. Nonferrous Met. Soc. China* **17**, 58 (2007).